Computational analysis of aortic hemodynamics - comparison of outflow modelling strategies

Laura Sumares Velosa Barreto

Instituto Superior Técnico, Universidade de Lisboa

November 2019

Abstract

Cardiovascular diseases have been reported, for the last 15 years, the leading cause of death, by the World Health Organization. However, the majority of these conditions are preventable if we improve our knowledge of the cardiovascular system and use it to create computational fluid dynamic models that can be used to predict hemodynamic metrics and associate them physiological and pathologic cases. The scientific community is committed to model the entire cardiovascular system, nonetheless, due to its complexity, it is common to model solely a portion of the cardiovascular system and represent the remaining circulation through boundary conditions (BCs). Therefore, the employment of appropriate BCs determines the computational accuracy of the numerical simulation.

This work focused on determining the variations in hemodynamic performances caused by different BCs imposed on the secondary outlets that branch from the aortic arch. Those conditions were: traction-free, flow ratio based on Murray's Law and flow ratio based on literature percentages. To achieve so, a thoracic aorta was modeled from the segmentation of CT-images and defined as the computational domain where the Navier-Stokes equations were solved by the Finite Element Method. At the inlet, the imposed BC was the subject-specific ascending aorta flow, obtained from ultrasound Doppler measurements and at the main outlet a traction-free BC was imposed. The results of the simulations were compared in terms of velocity and wall shear stress distribution and flow profiles and validated against subject-specific flow rate. The results were most consistent with the clinical observations in the simulations where flow fraction was imposed, while the simulation in which traction-free was imposed presented some singularities.

Keywords: cardiovascular system, thoracic aorta, hemodynamics, computational fluid dynamics, boundary conditions, numerical simulation.

Introduction

Over the last 15 years, cardiovascular diseases have been reported as the global leading cause of death.[1] Undoubtedly, these numbers raise concern, and even though the risk factors of these conditions have been identified, there is a demand from the medical community for scientifically rigorous and quantitative research. Comprehension of the cardiovascular system through the application of mathematical models, aligned with accurate numerical algorithms, has been progressing over the years[2]. The numerical methods for solving fluid dynamics problems are known as computational fluid dynamics (CFD) methods. Particularly, the alignment between these and the cardiovascular system, seeks to explain the physical laws that govern the flow of blood, in other words, the dynamics of blood flow (hemodynamics). Numerical description helps us quantifying parameters, such as pressure, flow velocity and orientation or forces applied in the vessels, that characterize the physiological and pathological states. This knowledge can be used to investigate and explain pathologies, and further, predict outcomes and have meaningful clinical applications, for instance, helping surgeons understand how different surgical solutions might impact the blood circulation.

The first step on simulating blood flow is to obtain the geometry, or physical bounds of the vessel. Fluid dynamical problems are often conceptualized in unbounded domains[3], however, the cardiovascular system has millions of blood vessels[4], a number that increases the complexity of the

model and the computational cost of such simulation. Therefore, most methods of numerical simulation require a truncation of the conceptual domain to a bounded one, introducing artificial boundary conditions. The boundary conditions (BCs) represent interactions with the upstream and downstream vasculatures absent in the computational domain of interest. For that reason, physiologically accurate BCs that are robust, as well as simple to implement, must be carefully considered for each problem, to ensure they replicate with a high degree of accuracy the real hemodynamics.

Ideally, the BC should incorporate patient-specific data (ex. velocity or flow rate)[5], obtained from non-invasive *in vivo* measurements. However, these measurements are not always possible to retrieve, especially if we think about the number of inlets and outlets the cardiovascular system has[6].

The inlet boundary conditions should represent the vasculature upstream the vessel of interest. The simplest alternatives include idealized velocity profiles, which are supported by clinical evidence, for instance, flat-velocity, fully-developed or Womersley profiles[7,8]. When time-varying velocity data obtained with PC-MRI (Phase-contrast Magnetic Resonance imaging) or Ultrasound are available, an average velocity can be prescribed to the inlet[7]. Additionally, if the diameter of the section where the velocity is obtained is measured, the volumetric flow rate can also be prescribed as the inlet boundary condition[8-10] according to (1):

$$Q[m^3/s] = v[m/s] \times A[m^2] \quad (1)$$

where Q is the volumetric flow rate, v is the measured average velocity and A is the area of the section where the velocity profile was measured. Less frequently prescribed[11], patient-specific time-varying pressure waveforms are also available, usually from catheterization-based pressure acquisition, which is an invasive and painful technique only performed in patients with indication for surgery.

Despite the importance of the inlet boundary condition, the solutions to the simulations in large arteries are also highly dependent on the imposed outlet boundary conditions to represent the downstream microvascular systems. According to Xu et al.[12], in the situation where patient-specific flow measurements are unavailable, constant fractions of the inflow are prescribed as outflow BCs. Such fractions are commonly approximated according to Murray's Law[5,6,13], or according to a reference flow percentage.

However, it is still common amongst the cardiovascular research community to use simpler outlet boundary conditions such as traction free, which consists in assigning a zero pressure to the boundary, similar to assuming the vessel is cut and exposed to atmospheric conditions, thus neglecting the resistive effects of downstream vessels.

For inlets and outlets, there are also more complex zero-dimensional or one-dimensional methods that attempt to capture the resistance of proximal and distal arteries, as well as the capacitance of the downstream vasculature[6,8]. Unfortunately, the parameters that govern these models, like resistances and compliances, can hardly be obtained from measurements or other means and rely on accurate pressure measurements in the proximal aorta (which, as referred, are very unlikely to obtain). In addition, due to multiple physiological states, there is not one correct resistance value, for example. Therefore, the parameters of such models must be tuned to approximate the measured data, using iterative mathematical methods, that themselves are complex and time-consuming. Despite the ability to study the interactions between the heart and the arterial system, these methods still need improvements, namely automatic optimization of these parameter values[8,15].

There appears to be a lack of comparison between the effects of outlet BCs based on zero pressure, flow ratios based on Murray's Law, and flow ratios based on literature percentage in a realistic human thoracic aorta (TA) model and in a pulsatile regime[5,7]. Therefore, the aim of this project is to compare the impact of using these simple, but common, outlet BCs on various hemodynamic metrics on a complex human aortic model where the inlet BC is the subject-specific flow rate. Section 2 presents the steps taken to describe the domain, the solving methodology and implementation. The obtained results for velocity (its surface distribution and streamline representation), flow and wall shear stress (WSS) fields are introduced and discussed in section 3. Finally, section 4 presents the main conclusions obtained in this work.

Methods

Model description

The precise geometry of a human thoracic aorta is studied. It was obtained from computed tomography (CT) images, acquired with a contrast agent of iopromide, kindly ceded from Hospital Santa Marta (Lisbon). To make a 3D reconstruction of the lumen of the aorta, all DICOM slices from the raw medical images were processed by 3D Slicer, and the aorta was segmented from the remaining structures present in the CT. The final reconstructed model covered the thoracic aorta, starting at the ascending aorta, including the major side branches visible in the images: brachiocephalic artery (BA), left common carotid artery (LCA) and left subclavian artery (LSA). The portion of the arteries included in the geometrical model was determined by the quality of the images. The segmented model was smoothed in the software MeshLab with the Taubin smoothing method and the applied parameters, λ, μ and smoothing steps (number of iterations) were, respectively, 0.70, -0.71 and 100[16]. Following, the Vascular Modelling Toolkit, vmtk, was the system used to clip the end caps and create the vessel wall. The resulting model was then converted to a compatible format and imported to COMSOL Multiphysics. The complete physical description of the model comprehended six boundaries, corresponding to the inlet (in the ascendant portion of the aorta), the main outlet (in the descendent portion of the aorta) and the three secondary outlets: BA, LCA and LSA.

The CFD problem was modelled using (2) and (3), the incompressible Navier-Stokes equations, which were solved in the computational domain.

$$\nabla \cdot u = 0 \tag{2}$$

$$\rho\left[\frac{\partial u}{\partial t} + (u \cdot \nabla)u\right] = -\nabla p + \mu\nabla^2 u \tag{3}$$

The principal quantities that describe blood flow are the velocity vector u = [*u, v, w*] and the pressure p, that vary in space *x,y,z* and time t. The term $\nabla \cdot u$ is the spatial divergence of the vector field u and ρ is the fluid's density. Blood was considered a Newtonian fluid, a commonly accepted assumption for flow in the aorta[5,6,12,17-19] with a density of 1060 kg/m³ and a dynamic viscosity of 0.004 Pa·s.

At the vessel wall, a no-slip boundary condition was imposed, u = 0, which means the velocity of the elements of the wall was set to zero. It also implies that the velocity of the fluid will tend to zero at the lumen-wall interface.

At the inlet, a patient-specific flow rate, Q_i, obtained from Doppler measurements of the velocity at a section of the ascending aorta, v_i, and the area of that section, A_{inlet}, was imposed. It is described by (4):

$$Q_i = v_i \times A_{inlet} \tag{4}$$

At the main outlet, in the descending aorta, the boundary condition imposed was traction-free. Mathematically, this is a pressure condition that specifies the normal stresses at the boundary, which are approximately equal to the pressure, are zero. The tangential stress component is also set to 0 Pa therefore, the equation used to apply this BC was:

$$\left[-pI + \mu\left(\nabla u + (\nabla u)^{T}\right)\right]n = -P_0 n \tag{5}$$

The boundary conditions applied to the secondary outlets were different for the three cases studied. In the first test case studied, the boundary conditions for the secondary outlets (BA, LCA and LSA) were set as traction-free. Therefore, the definition of each of these boundaries was the same as that of the outlet at the descendent aorta.

In the second test case studied, Murray's Law based flow ratio was imposed to each secondary outlet. Murray's law states that the flow in a vessel is proportional to the diameter of the vessel lumen

cubed therefore, the flow ratio assigned to an outlet boundary can be determined with respect to the inlet flow rate through the relation:

$$\frac{Q_o}{Q_i} = \frac{D_o^3}{D_i^3} \tag{6}$$

where Q_o is the flow through BA, LCA or LSA, Qi is the flow through the inlet, D_o is the diameter of BA, LCA or LSA and D_i is the diameter of the inlet.

The third test case consisted in assigning flow percentages to the secondary outlets of the aorta. Following the references, the percentage of the flow rate for each secondary branch is of 5%[10,14]. Therefore, to each outlet, BA, LCA and LSA, expression (7) was imposed.

$$Q_o = Q_i \times 0.05 \tag{7}$$

The system was discretized in time with the Backward Differentiation Formula (BDF) of order 1 and 2. The space discretization was performed with the Finite Element Method (FEM). The resulting system of equations was solved in COMSOL Multiphysics.

Computational implementation

To impose the inflow, the software considers a virtual domain that is an extrusion of the inlet. The boundary condition applied, expression (8), uses the assumption that the flow in this virtual domain is fully developed laminar flow.[23] The wall of this domain, with length L_{entr}, inherits the conditions from the real domain. The length of this virtual extension is determined experimentally, in order to have a fully-developed flow by the time it reaches the real inlet. The software also adds and ODE to calculate the pressure applied at the entrance of this virtual extension, p_{entr}, such that desired inlet flow rate is obtained.

$$L_{entr}\nabla_t \cdot \left[-pI + \mu\left(\nabla_t u + (\nabla_t u)^{\top}\right)\right] = -p_{entr}n \tag{8}$$

To impose the traction-free BCs, the software uses equation (4) and adds an equation that reflects the *Suppress backflow* method from COMSOL. Expressions in (9) mean that the software is free to adjust the outlet pressure P locally, in order to prevent fluid from exiting the domain through the boundary. Effectively, it means that the prescribed pressure P is P_0 if $u \cdot n \geq 0$, but it becomes smaller at locations where $u \cdot n < 0$. Sometimes it becomes smaller, and the backflow is substantially reduced, but not enough to prevent fluid from entering the domain through the boundary.

$$\begin{gathered}\left[-pI + \mu\left(\nabla u + (\nabla u)^{\top}\right)\right]n = -Pn \\ P \leqslant P_0\end{gathered} \tag{9}$$

Regarding the outflow conditions, analogously to the inflow, COMSOL Multiphysics also considers an extrusion of the outlet with length L_{exit} as virtual domain attached to it. The pressure p_{exit} is applied at the exit of the virtual extension and computed by and ODE added by the software to ensure the outlet flow rate is obtained. The expression imposed was:

$$L_{exit}\nabla_t \cdot \left[-pI + \mu\left(\nabla_t u + (\nabla_t u)^{\top}\right)\right] = -p_{exit}n \tag{10}$$

To conclude the problem formulation, the solving methods were defined for the simulation of 1.2 s, which is the period of two cardiac cycles. The BDF with variable order, implemented by COMSOL, was allowed to change between 1 and 2, and had variable step-size constrained to a maximum of 0.001. This means that the software would automatically adjust the time step size in order to maintain the desired *Relative Tolerance.* In this method, when it starts, the solver estimates an initial time step size upon the total simulation time. During the resolution, if there are any fast variations in the solution, the solver will automatically take smaller time steps, as needed. Analogously, it will take larger time steps when the solution is only varying gradually. The exact version of the BDF order corresponds to what was described in Hindmarsh et al [21].

For each time step the FEM is used to discretize the space. The discretization of the fluid was set to P1+P1, that is the polynomials chosen to interpolate the velocity and pressure over the elements are of first order. Linear elements are computationally cheaper (the element order directly affects the number of degrees of freedom in the solution[22]). However, the Navier-Stokes equations are unstable when using P1+P1 discretization therefore, undershoots and overshoots can occur in the numerical solution at sharp gradients. COMSOL Multiphysics addresses these oscillations by Consistent Stabilization methods, namely Streamline diffusion and Crosswind diffusion.

Still regarding space, the finite element mesh size was carefully selected as a trade-off between accuracy and computational cost. Thus, a mesh convergence analysis was performed, comparing the absolute and relative error of the velocity according to L2- and H1-norms, of 5 mesh sizes. The refinement study concluded that the mesh of 9×10^{-4} m characteristic size was the best suited, consisting of 775733 degrees of freedom. This mesh was composed of free tetrahedral elements and three boundary layers, which reflects in increased element density close to the wall.

At last, each iteration was solved with a Fully Coupled approach, which means equations (2) and (3), discretized in time, were solved at the same time. The resulting system is non-linear and solved with the Newton Method. This means that the time dependent solver computes the solution to the nonlinear system of equations at each time step via a set of iterative techniques based on Newton's method. This method evaluates a function, as well as its derivative, the Jacobian, at every time step. The Jacobian is relatively expensive to compute therefore, the Jacobian update was set to once per time step. At each iteration, the linearized system was solved using the PARDISO direct method solver.

Results

The results of the three-simulations were compared in terms of velocity, flow and wall shear stress. The instances selected to show the results, t=0.85 s (accelerating phase of systole), t=0.945 s (peak of systole) and t=1.02 s (decelerating phase of systole), were chosen because of their significative relevance, compared to the diastole, where the values are of the velocity are closer to zero.

Velocity and Streamlines

Figure 1 shows the distribution of streamlines during systole, coloured according to the magnitude of the velocity. These result from the integration of velocity vectors and show the direction in which a fluid element will travel at any point in time. In the three cases, at the ascending aorta a fully-developed flow is observed, slightly skewed, with higher velocities along the concavity. On the wall, the velocity is zero, as imposed by the no-slip condition. At the 180-degree turning of the aortic arch, the non-uniform flow is forced to turn, and the fluid particles are forced to change direction and accelerate in order to preserve the axial flow. As the initial flow is fully developed, the highest velocities in the centre have high inertia, therefore are not easily deflected. In turn, the blood near the wall has less inertia thus, greatly displaced. As a consequence, after the bending, the highest velocities are found closer to the outer wall of the curvature. These deflected velocities generate rotational components of the velocity. Still at the systolic peak, studies reported that highest to lowest velocities are seen in the descending aorta, then in the thoracic aorta and ascendant aorta, in this order[20]. Test B and C are in accordance to these findings however, test A is not. The velocity is higher at the secondary branches, which might be justifiable by the dependence on the relative distance to the inlet sections, due to the imposed pressure difference[3].

Additionally, significant recirculation of blood flow is observed right after the curvature. However, this is micro-recirculation, at negligible velocities. Since streamlines are the integration of the velocity vectors, they capture their direction, even if it is the direction of residual velocity.

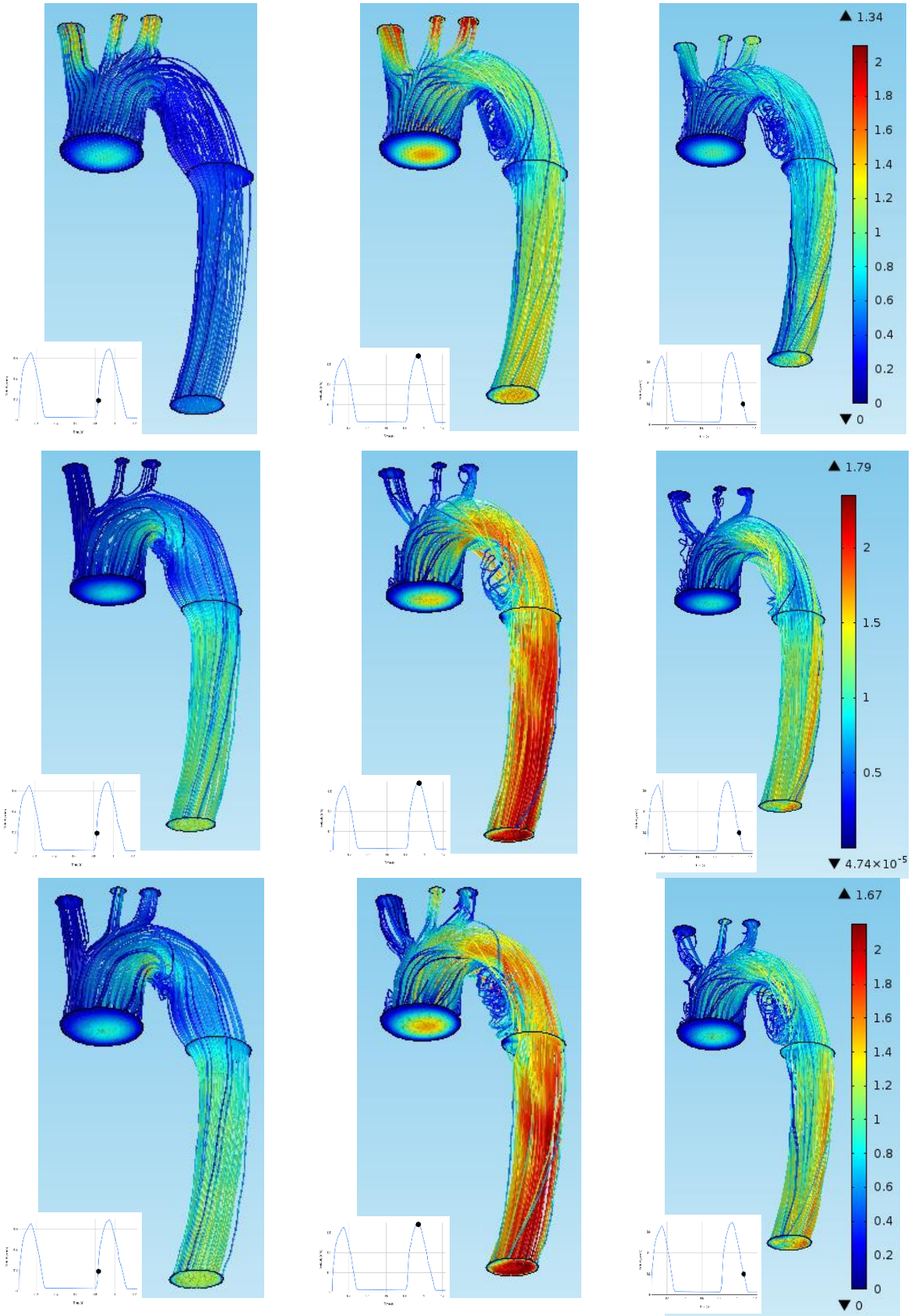

Figure 1: Streamline plots on the fluid domain, computed from test A, B and C presented in the first, second and third rows, respectively, at time instances 0.85 s, 0.945 s and 1.02 s presented in the first, second and third columns, respectively. The streamlines have a colour expressing the velocity magnitude in m/s.

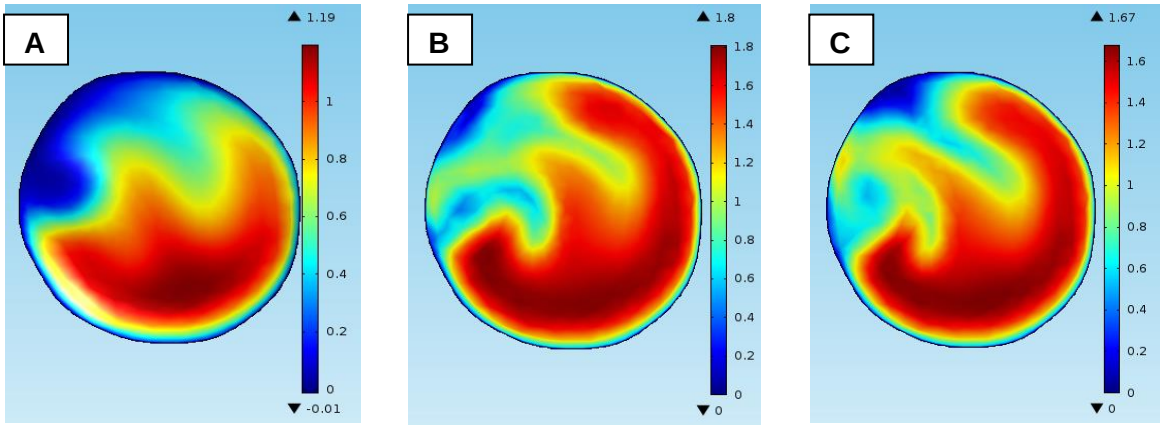

Figure 2: Distribution of velocity magnitude on the TA cross-section, computed from test A, B and C at systolic peak. Scale units: m/s.

Special attention is given to systolic peak as Figure 2 shows the distribution of velocity at a cross-section at the thoracic level, after the bending of the vessel, where a characteristic crescent-shaped axial velocity profile is observed. This profile reflects the rotational components of the velocity that arise from the bending. Each case in this figure is represented according to its own scale, in order to enhance the velocity profile. As previously observed in Figure 1, the values of velocity are higher in tests B and C than A.

Wall Shear Stress (WSS)

Wall shear stresses are the superficial forces that develop tangentially to the vessel wall because of blood flow. This quantity is computed from (11):

$$\mathrm{WSS} = \sigma - \sigma \cdot \mathrm{n} \tag{11}$$

Where σ is the total stresses developed, in both tangential and normal direction, computed from:

$$\sigma = \left[-\mathrm{pI} + \mu\left(\nabla \mathrm{u} + (\nabla \mathrm{u})^{\mathrm{T}}\right)\right]\mathrm{n} \tag{12}$$

where μ is the viscosity and the term in brackets, the gradient of the velocity, is the shear strain rate.

Throughout the cardiac cycle, the distribution of the magnitude of WSS seems to be highly correlated with the flow streamlines and respective velocity field.

Primarily, complex WSS fields are observed due to the complex flow structures. However, common aspects were found between the three test cases, that is, the location of the highest shear stresses. At the aortic arch, there are extraordinary WSS peaks at the base of the branches, which can be comprehended as bifurcations. Because of them, when blood arrives to the aortic arch, it is forced to divide in the branches. However, due to its high inertia, it cannot be immediately displaced into the axial directions of the branches. Consequently, the flow moves next to the inner walls of the bifurcation, developing high shear stresses on the flow divider, as observed in Figure 3. Furthermore, in test A, high WSS exist along the secondary branches, not just at their base, due to the high velocities that develop there, as seen in Figure 1.

Secondly, as a consequence of the asymmetry of the initial flow, which is skewed to the inside of the curvature of the vessel, at the aortic arch, the change in the direction of velocity implies that high shear stress develops on the outer wall of the curvature, and low shear stress on the inner wall.

Additionally, there are WSS peaks detected in the apex of the curve of the aortic arch. These may be an overestimation resultant for any error in the geometry, and it has been reported in previous studies[17].

Validation

The results for the flow, computed as the solution of the three test cases is compared with the measured flow of the patient. In Figure 4, the described results are presented for the section in the thoracic aorta, along with the relative error of each test case. The relative error is computed, at each time instance, from the following expression:

$$e^{rel} = \frac{\|f_i - f_m\|}{\|f_m\|} \tag{13}$$

where f_m is the value of the measured flow, and f_i is the computed flow, from the three solutions, i = A, B, C.

It is clear, observing the graphic on top of Figure 4, that in the simulation where traction-free was imposed to the secondary outlets, the flow through the TA section is far from the expected, in comparison with the solutions from inflow dependent methods. In the bottom graph of the same figure, the relative errors are presented. As expected, the highest absolute relative value is associated with the simulation of test A. As for the other two, despite the maximum relative error of test B is higher than that of test C, in the remaining time instances, the relative errors of the former are always lower than those of the later. Therefore, for the representation of the flow across the TA section, the flow fraction based on Murray's Law is the preferred outlet boundary condition for the secondary outlets.

Conclusions

The numerical simulations in this paper have been made in one of the most complex anatomies of the cardiovascular system, the thoracic aorta, with branching, tapering of lumen and curvature in aortic arch. The velocity distribution verified that these results met the theoretical proposition and agree with previously reported results. The main difference in velocity distribution was found at the secondary outlets, where the traction-free boundary condition resulted in a flat high-speed profile, similar for the three branches, whereas the inflow fraction boundary condition resulted in fully developed flows and lower velocities. Even though, these disparities in the aortic branches seem to not have affected the velocity distribution in the rest of the fluid domain and it has been shown that the distribution of the flow in the secondary branches has a weak impact on the hemodynamic parameters[18]. The WSS magnitude distribution showed consistent results between simulations and with the theory except, again, for the aortic branches of traction-free imposition test. While the three outflow conditions could not perfectly reproduce the flow profile as measured, they still showed good agreement with the measured results and expected velocity and WSS distribution. Simulations where flow fraction of the inflow were imposed at the secondary outlets were most consistent with the clinical observations, while the simulation where a traction-free boundary condition was imposed presented some singularities.

Limitations & Further work

The use of CFD has limitations primarily related to the model assumptions that are made when these simulations are performed, for example in the geometry of the vessel (the accuracy of the image acquisition can be questioned), for viscosity of blood, distensibility of the vessel wall or in the flow conditions (for instance, one could question if the division of flow through the branches is constant throughout the cardiac cycle).

A more realistic approach would be to use PC-MRI to measure velocity profile at the root of the aorta, which could give velocity vector information accounting for helical flow or other effects. The same goes for the outlets, once this information would be useful to validate the results.

Furthermore, a future direction of this work should involve comparing these simple and commonly used boundary conditions against more advanced outlet boundary condition models, and asses their accuracy versus computational cost, to help future researchers.

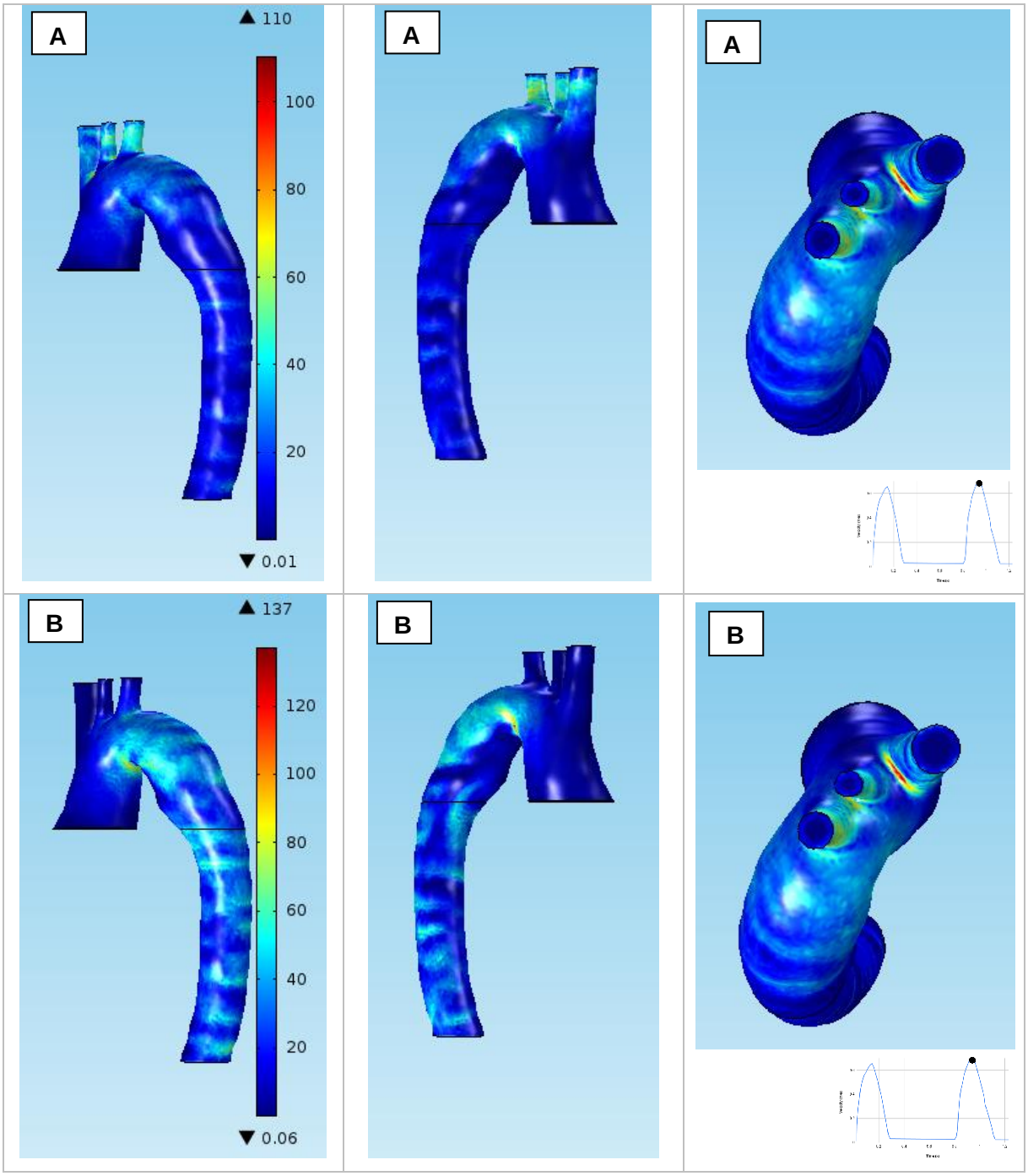
A
▲ 110
100
80
60
40
20
▼ 0.01
A
A
B
▲ 137
120
100
80
60
40
20
▼ 0.06
B
B

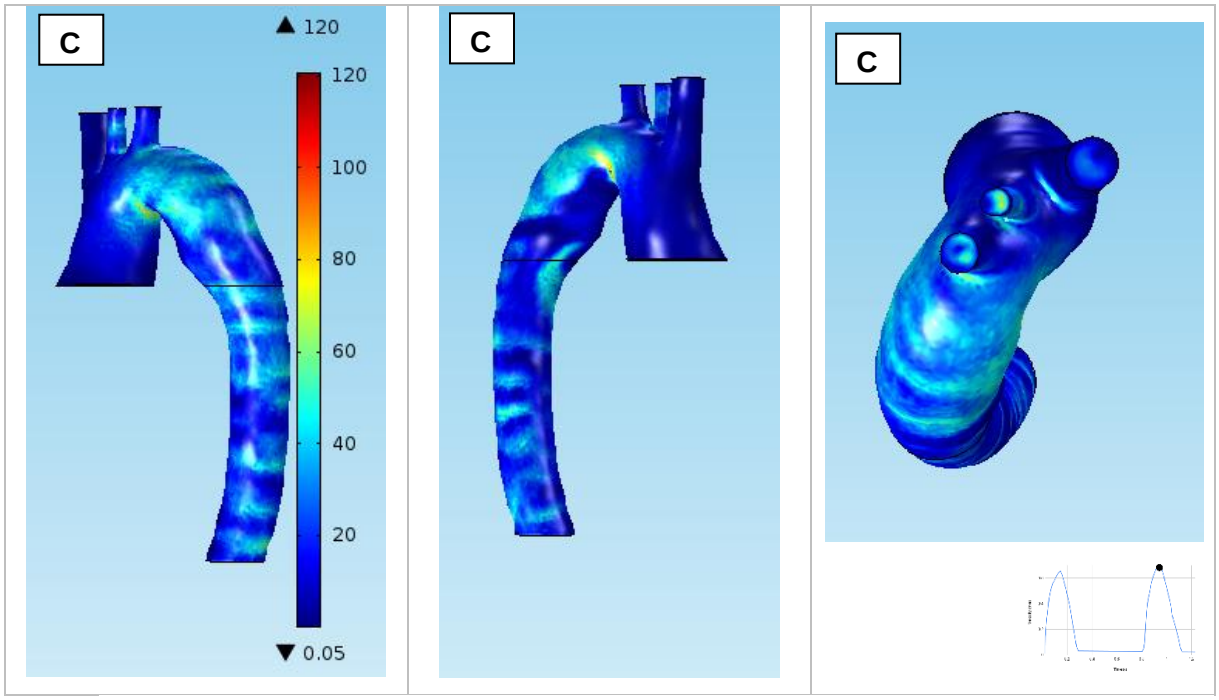

Figure 3: WSS for systolic peak, at t=0.945 s. Solution of test cases A, B and C presented in the first, second and third rows. First column shows and anterior view, second column shows a posterior view and third column shows a superior view. Scale units: Pa. [First part of the figure is in the previous page and corresponds to tests A and B]

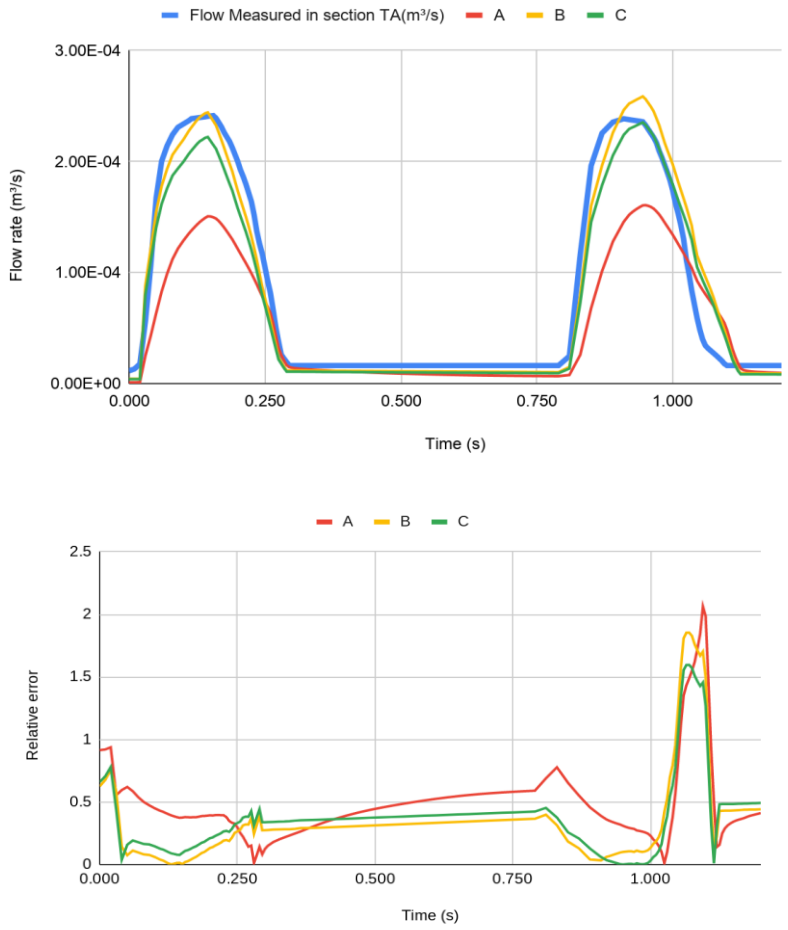

Figure 4: Top: Comparison between measured and computed flow rates in section TA [m³/s]. Bottom: Comparison between the relative errors associated with the computed flow rates.

References

[1] World Health Organization – The top 10 causes of death. (n.d.). http://www.who.int/news-room/fact-sheets/detail/the-top-10-causes-of-death [accessed July, 2019]

[2] Quarteroni, A. (2006) What Mathematics can Do for the Simulation of Blood Circulation, AMS Subject Classification: 92C50, 96C10, 76Z05, 74F10, 65N30, 65M60

[3] Heywood, J. G., Rannacher, R., & Turek, S. (1996) Artificial Boundaries And Flux And Pressure Conditions For The Incompressible Navier-Stokes Equations. International Journal for Numerical Methods in Fluids, 22(5), 325–352. doi: 10.1002/(sici)1097-0363(19960315)22:5<325::aid-fld307>3.0.co;2-y

[4] The Editors of Encyclopaedia Britannica. (2019) Blood vessel. Retrieved from https://www.britannica.com/science/blood-vessel. [accessed July 2019]

[5] McElroy, M., & Keshmiri, A. (2017) Impact of Using Conventional Inlet/Outlet Boundary Conditions on Haemodynamic Metrics in a Subject-Specific Rabbit Aorta. Proceedings of the Institution of Mechanical Engineers, Part H: Journal of Engineering in Medicine, 232(2), 103–113. doi: 10.1177/0954411917699237

[6] Xu, H., Piccinelli, M., Leshnower, B. G., Lefieux, A., Taylor, W. R., & Veneziani, A. (2018) Coupled Morphological–Hemodynamic Computational Analysis of Type B Aortic Dissection: A Longitudinal Study. Annals of Biomedical Engineering, 46(7), 927–939. doi: 10.1007/s10439-018-2012-z

[7] Caballero, A. D., & Laín, S. (2013) A Review on Computational Fluid Dynamics Modelling in Human Thoracic Aorta. Cardiovascular Engineering and Technology, 4(2), 103–130. doi: 10.1007/s13239-013-0146-6

[8] Kim, H., Figueroa, C., Hughes, T., Jansen, K., & Taylor, C. (2009) Augmented Lagrangian method for constraining the shape of velocity profiles at outlet boundaries for three-dimensional finite element simulations of blood flow. Computer Methods in Applied Mechanics and Engineering, 198(45-46), 3551–3566. doi: 10.1016/j.cma.2009.02.012

[9] Doormaal, M. A. V., Kazakidi, A., Wylezinska, M., Hunt, A., Tremoleda, J. L., Protti, A., … Ethier, C. R. (2012) Haemodynamics in the mouse aortic arch computed from MRI-derived velocities at the aortic root. Journal of The Royal Society Interface, 9(76), 2834–2844. doi: 10.1098/rsif.2012.0295

[10] Tse, K. M., Chang, R., Lee, H. P., Lim, S. P., Venkatesh, S. K., & Ho, P. (2012) A computational fluid dynamics study on geometrical influence of the aorta on haemodynamics. European Journal of Cardio-Thoracic Surgery, 43(4), 829–838. doi: 10.1093/ejcts/ezs388

[11] Vasava, P., Jalali, P., Dabagh, M., & Kolari, P. J. (2012) Finite Element Modelling of Pulsatile Blood Flow in Idealized Model of Human Aortic Arch: Study of Hypotension and Hypertension. Computational and Mathematical Methods in Medicine, 2012, 1–14. doi: 10.1155/2012/861837

[12] Xu, P., Liu, X., Zhang, H., Ghista, D., Zhang, D., Shi, C., & Huang, W. (2018) Assessment of boundary conditions for CFD simulation in human carotid artery. Biomechanics and Modeling in Mechanobiology, 17(6), 1581–1597. doi: 10.1007/s10237-018-1045-4

[13] Trachet, B., Bols, J., Santis, G. D., Vandenberghe, S., Loeys, B., & Segers, P. (2011) The Impact of Simplified Boundary Conditions and Aortic Arch Inclusion on CFD Simulations in the Mouse Aorta: A Comparison With Mouse-specific Reference Data. Journal of Biomechanical Engineering, 133(12). doi: 10.1115/1.4005479

[14] Liu, X., Fan, Y., Deng, X., & Zhan, F. (2011) Effect of non-Newtonian and pulsatile blood flow on mass transport in the human aorta. Journal of Biomechanics, 44(6), 1123–1131. doi: 10.1016/j.jbiomech.2011.01.024

[15] Creigen V., Ferracina L., Hlod A., Mourik S.V., Sjauw K., Rottschafer V., Vellekoop M., Zegeling P. (2007) Modeling a Heart Pump.

[16] Taubin, G. (1995) Curve and surface smoothing without shrinkage. Proceedings of IEEE. 852-857.

[17] Reymond, P., Crosetto, P., Deparis, S., Quarteroni, A., & Stergiopulos, N. (2013) Physiological simulation of blood flow in the aorta: Comparison of hemodynamic indices as predicted by 3-D FSI, 3-D rigid wall and 1-D models. Medical Engineering & Physics, 35(6), 784–791. doi: 10.1016/j.medengphy.2012.08.009

[18] Assemat, P., Armitage, J. A., Siu, K. K., Contreras, K. G., Dart, A. M., Chin-Dusting, J. P., & Hourigan, K. (2014) Three-dimensional numerical simulation of blood flow in mouse aortic arch around atherosclerotic plaques. Applied Mathematical Modelling, 38(17-18), 4175–4185. doi: 10.1016/j.apm.2014.01.004

[19] Tagliabue, A., Dedè, L., & Quarteroni, A. (2017) Fluid dynamics of an idealized left ventricle: the extended Nitsches method for the treatment of heart valves as mixed time varying boundary conditions. International Journal for Numerical Methods in Fluids, 85(3), 135–164. doi: 10.1002/fld.4375

[20] Segadal, L., & Matre, K. (1987) Blood velocity distribution in the human ascending aorta. Circulation, 76(1), 90–100. doi: 10.1161/01.cir.76.1.90

[21] Hindmarsh, A., Brown, P., Grant, K., Lee, S., Serban, R., Shumaker, D., Woodward, C. (2005) Sundials: Suite of non-linear and differential/algebraic equation solvers. ACM Trans Math Softw. 31(3):363-396.

[22] COMSOL, Inc. (2014) COMSOL Multiphysics 5.0 Reference Manual.

[23] COMSOL, Inc. (2014) COMSOL Multiphysics 5.0 – The CFD Module Users Guide.